

# Delineating the role of ripples on thermal expansion of honeycomb materials: graphene, 2D-h-BN and monolayer(ML)-MoS<sub>2</sub>

P. Anees\*

Materials Physics Division, Indira Gandhi Centre for Atomic Research, HBNI, Kalpakkam 603 102, Tamil Nadu, India

M. C. Valsakumar†

Department of Physics, Indian Institute of Technology Palakkad, Palakkad 678 557, Kerala, India

B. K. Panigrahi

Materials Physics Division, Indira Gandhi Centre for Atomic Research, HBNI, Kalpakkam 603 102, Tamil Nadu, India‡

(Dated:)

We delineated the role of thermally excited ripples on thermal expansion properties of 2D honeycomb materials (free-standing graphene, 2D h-BN, and ML-MoS<sub>2</sub>), by explicitly carrying out three-dimensional (3D) and two-dimensional (2D) molecular dynamics simulations. In 3D simulations, the in-plane lattice parameter ( $\mathbf{a}$ -lattice) of graphene and 2D h-BN shows thermal contraction over a wide range of temperatures and exhibits a strong system size dependence. The 2D simulations of the very same system show a reverse trend, where the  $\mathbf{a}$ -lattice is expanding in the whole computed temperature range. Contrary to graphene and 2D h-BN, the  $\mathbf{a}$ -lattice of ML-MoS<sub>2</sub> shows thermal expansion in both 2D and 3D simulations and their system size dependence is marginal. By analyzing the phonon dispersion at 300 K, we found that the discrepancy between 2D and 3D simulations of graphene and 2D h-BN is due to the absence of out-of-plane bending mode (ZA) in 2D simulations, which is responsible for thermal contraction of  $\mathbf{a}$ -lattice at low temperature. Meanwhile, all the phonon modes are present in 2D phonon dispersion of ML-MoS<sub>2</sub>, which indicates that the origin of ZA mode is not purely due to out-of-plane movement of atoms and also its effect on thermal expansion is not significant as found in graphene and 2D h-BN.

## I. INTRODUCTION

Graphene has got enormous attraction due its fascinating electronic, thermal and mechanical properties<sup>1-3</sup>, and it is proposed as a promising candidate for next generation electronic industry<sup>1,4,5</sup>. The major pitfall in graphene based electronics is the absence of finite band gap in its electronic band structure. After successful isolation of graphene, the search for other 2D honeycomb materials were geared up in past few years. The 2D hexagonal (h)-BN, which is isostructural to graphene, is an insulator with a finite band gap  $\sim 5-6$  eV<sup>6</sup>, and exhibits intriguing electronic properties<sup>6-8</sup>. The family of 2D materials are getting richer day by day<sup>9</sup>. Apart from graphene and h-BN, monolayer(ML)-MoS<sub>2</sub> is another high interesting 2D honeycomb material<sup>10,11</sup>. ML-MoS<sub>2</sub> is a direct band gap<sup>10</sup> (1.9 eV) semiconductor, and it exhibits high photoluminescence yield<sup>12</sup>, which puts this material in the front-end of optoelectronic industry. The ML-MoS<sub>2</sub> based field effect transistors (FETs) shows high carrier mobility<sup>13</sup> and on/off ratios<sup>13-15</sup>.

Structural stability of the 2D crystals was an old dispute in condensed matter theory. According to Mermin-Wagner theorem<sup>16</sup>, the long wavelength thermal fluctuations will destroy the long-range order in 2D crystals. But in the case of graphene and 2D h-BN, these fluctuations are suppressed by strong anharmonic coupling between in-plane stretching and out-of-plane bending modes, leading to height fluctuations on the surface, known as ripples<sup>17</sup>. These intrinsic ripples are inevitable in 2D crystals, and they stabilizes the

2D membranes<sup>17-19</sup>. Transmission electron microscopic study reveals that, the suspended graphene sheets are not perfectly flat, they exhibits out-of-plane deformations<sup>20</sup>. Recent experiments using high resolution atomic force microscopy, shows sinusoidal ripples of periodicity 3 to 6 nm and amplitude of 10 to 100 pm on the surfaces of graphene and 2D h-BN layer of supported flakes<sup>21</sup>. The ripples structure in graphene could be manipulated to sketch devices based on local strain<sup>22</sup> and band gap engineering<sup>23</sup>.

For aforementioned applications of 2D materials, knowledge of linear thermal expansion coefficients (LTECs) is essential. Several studies has been reported the LTEC of graphene both from simulations<sup>18,24-27</sup> and experiments<sup>28-31</sup>. Mounet and Marzari<sup>24</sup> predicts that the LTECs of graphene remains to be negative upto 2300 K using quasi-harmonic calculations. Zakharchenko *et al*<sup>25</sup> performed Monte-Carlo (MC) simulations and found that in-plane lattice parameter ( $\mathbf{a}$ -lattice) contracts with temperature upto  $T = 900$  K and further it expands. *Ab initio* molecular dynamics (MD) simulations by Pozzo *et al*<sup>26</sup> shows that the C-C distance increases with an increase in temperature for both supported and free-standing graphene; meanwhile the  $\mathbf{a}$ -lattice is found to be contracting with an increase in temperature (upto 2000 K) in free-standing graphene. The above discrepancies among the various simulations arises due to the difference in the incorporation of anharmonicity in those calculations, its effects are very strong in 2D crystals<sup>18</sup>. From the experimental front, Bao *et al*<sup>28</sup>, reported the negative thermal expansion of graphene in the temperature

range 200 K - 400 K. Later, Yoon *et al*<sup>30</sup>, also found that thermal expansion coefficient of graphene is negative in the above temperature range using temperature dependent Raman spectroscopy. The authors also observed the strain effect induced by substrate-layer interaction can alter the physical properties of graphene.

In quasi-harmonic approximation (QHA) the 2D sheets are considered to be flat, hence the effects of ripples cannot be incorporated in a direct manner. Moreover, within the *ab initio* frame work we cannot include more than few hundreds of atoms in the simulation cell, which seems to be in-adequate to incorporate the long wavelength ripples. From the experimental perspective, most of the measurements are made on graphene supported on a substrate or over a trench, such measurements are extremely challenging due to the strain effects, and may not be able to capture the intrinsic thermal expansion properties of free-standing graphene with ripples. Classical MD simulations can incorporate millions of atoms and also computation can be done with free-standing sheets contains all rippling effects, hence it will be an ideal choice to overcome the above limitations. The thermal expansion of graphene has been reported in various studies as mentioned above. However, the thermal expansion of 2D h-BN and ML-MoS<sub>2</sub> are not studied in detail, which is essential to devise hybrid nano-devices and hetero-structures<sup>9</sup>. The objective of the present paper is to understand the the role of ripples on thermal expansion properties of honeycomb materials explicitly. To delineate the role of ripples, we studied the the thermal expansions of very same system using three-dimensional (3D) and two-dimensional (2D) molecular dynamics (MD) simulations, the later cannot incorporate the effects ripples.

## II. COMPUTATIONAL METHODS

All simulations are done using classical MD simulation package LAMMPS<sup>32</sup>. To understand the role of ripples, we explicitly carried out 2D and 3D simulations of very same system at different temperatures. In 2D simulations, we arrested the motion of atom along the direction normal to the sheet and prevent the formation of thermally excited ripples using *fix enforce2d* command<sup>32</sup>. Ripples are naturally included in 3D simulations and leads to a corrugated surface instead of flat 2D sheet. Simulation cell of different sizes are used to incorporate the effects of long wavelength ripples. Periodic boundary conditions (PBC) are employed in all the three directions. To avoid the un-physical interactions between the periodic images, the sheets are stacked one above another with an additional vacuum separation of 15 Å. In this study, we employed empirical interatomic potentials (EIP) to model the interactions in honeycomb structures. We followed the same algorithm for both 2D and 3D simulations which is given below. Inorder to eliminate any residual stresses that could be present in the initial con-

figuration, the geometry is relaxed using conjugate gradient algorithm. The system is then equilibrated for 500 picoseconds (ps) in isobaric-isothermal (NPT) ensemble at desired temperatures and ambient pressure. After ensuring the proper equilibration and thermalization, we monitored the variation of lattice parameters as a function temperatures. The whole simulations are done for 3.2 nanoseconds. The linear thermal expansion coefficients (LTECs) are obtained by direct numerical differentiation (equation 1) of above data.

$$\alpha(T) = \frac{1}{a(T)} \frac{da(T)}{dT} \quad (1)$$

## III. RESULTS AND DISCUSSIONS

Figure 1 displays the configuration of graphene, 2D h-BN and ML-MoS<sub>2</sub> at 300 K. In 2D simulation, we obtained a flat 2D sheet without any ripples, while 3D simulation shows corrugations on the surface due to the formation of ripples. The interactions between C-C atoms in honeycomb lattice of graphene is modeled using a bond-order potential (LCBOP)<sup>33</sup>. The LCBOP potential predict the equilibrium in-plane lattice parameter (*a*-lattice)  $a_0 = 2.459$  Å, shows an excellent agreement with experiment ( $a_0 = 2.463$  Å). We used simulation cells of various sizes ( $10 \times 10 \times 1$ ,  $30 \times 30 \times 1$ ,  $50 \times 50 \times 1$ ,  $70 \times 70 \times 1$ ,  $100 \times 100 \times 1$ ,  $150 \times 150 \times 1$ ) to incorporate the effect of long wavelength ripples. Figure 2 displays the temperature dependence of *a*-lattice and linear LTEC of free-standing graphene. In 3D simulations, we found that the *a*-lattice decreases with an increase in temperature. Fourth order polynomial fit to the above data shows that minima occurs in the temperature range 1300 K - 1400 K, and further it expands with an increase in temperature, this is consistent with our previous study<sup>18</sup>.

Noteworthy, the temperature evolution of *a*-lattice is system size dependent (Figure 1). For simulation cell of size  $10 \times 10 \times 1$  (contains only 200 atoms) *a*-lattice shows relatively less contraction with respect to bigger cells and minima occurs around  $T = 1100$  K. As we increase the system size size, *a*-lattice shows a convergence from  $70 \times 70 \times 1$  (9800 atoms) onwards, and the minima falls in the temperature range 1300 K - 1400 K (dependence on system size). The similar system size dependence was reported by Pozzo *et al*<sup>26</sup>, where they used simulation cells of sizes  $8 \times 8 \times 1$ ,  $10 \times 10 \times 1$  and  $16 \times 16 \times 1$  contains 128, 200 and 512 atoms, respectively. Fasolino *et al*<sup>17</sup> observed fluctuations with wavelength of the order of 80 Å at 300 K from their Monte Carlo simulations. To incorporate such long wave length fluctuations bigger simulation cells are required, which makes *ab initio* Car-Parinello simulations prohibitive. In the present study, we used a simulation cell of size  $150 \times 150 \times 1$  (45000 atoms), which is capable of incorporating all long-wavelength rippling effects.

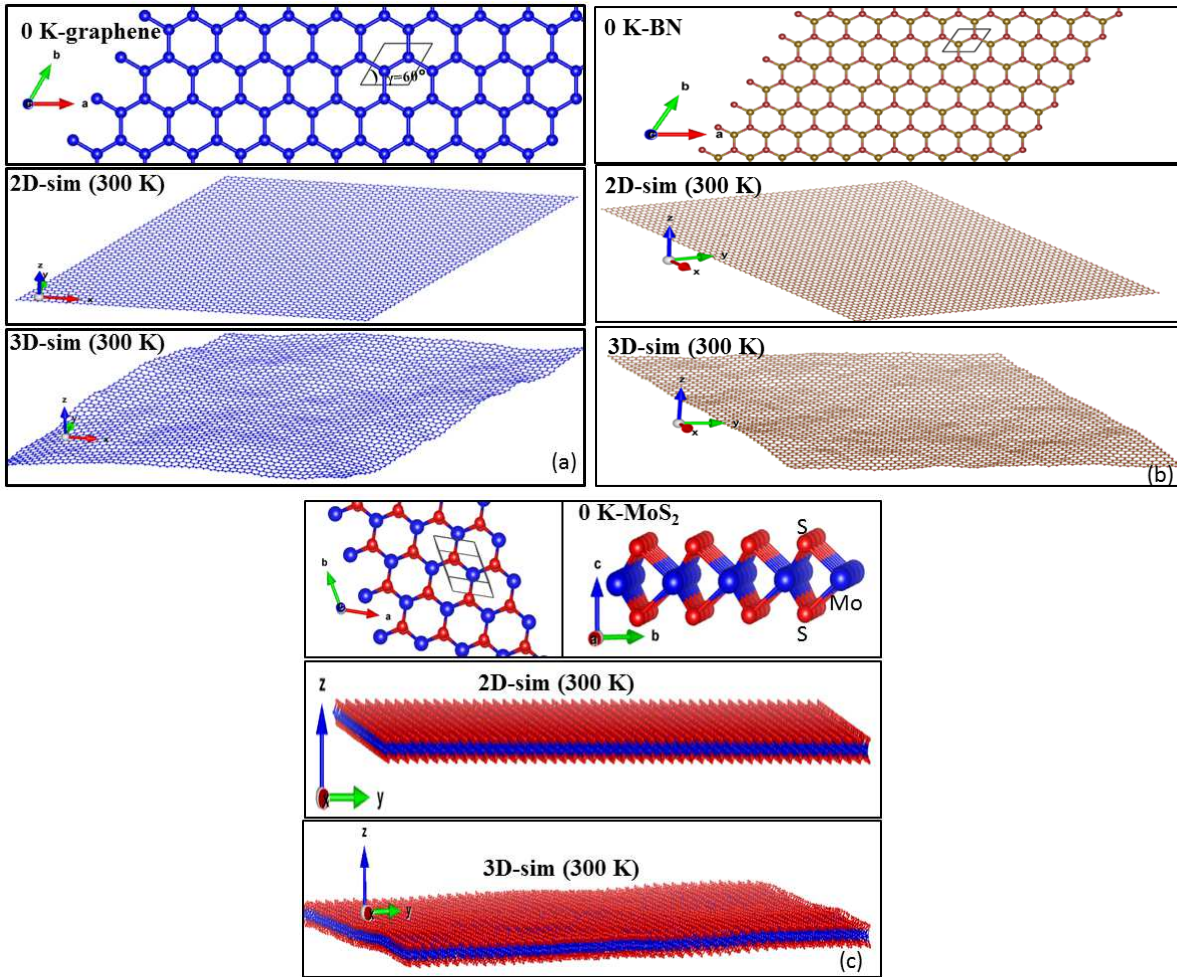


Figure 1. The 2D honeycomb lattices of (a) graphene, (b) 2D h-BN and (c) ML-MoS<sub>2</sub>. (top) The 2D sheets at 0 K, the unitcells can be represented using a rhombus, and the corresponding primitive translation vectors are  $\vec{a}=(a,0,0)$ ,  $\vec{b}=(a/2,\sqrt{3}a/2,0)$  and  $\vec{c}=(0,0,c)$ ; (middle) snapshots of sheets obtained from 2D simulations at 300 K. (bottom) sheets obtained from 3D simulation at 300 K, and they are no longer flat as in 2D simulations, the height fluctuation (ripples) normal to the surfaces are conspicuous.

| simulation cell size    | 2D simulation $\alpha_a (\times 10^{-6} K^{-1})$ | 3D simulation $\alpha_a (\times 10^{-6} K^{-1})$ | expt. $\alpha_a (\times 10^{-6} K^{-1})$                          |
|-------------------------|--|--|---|
| 10×10×1 (200 atoms)     | 5.178  | -2.499   | -5.500 <sup>a</sup> , -7.000 <sup>b,c</sup> , -8.000 <sup>d</sup> |
| 30×30×1 (1800 atoms)    | 5.226  | -4.095   |   |
| 50×50×1 (5000 atoms)    | 5.235  | -4.100   |   |
| 70×70×1 (9800 atoms)    | 5.230  | -4.380   |   |
| 100×100×1 (20000 atoms) | 5.243  | -4.350   |   |
| 150×150×1 (45000 atoms) | 5.241  | -4.524   |   |

Table I. The system size dependence of linear thermal expansion coefficients (LTECs) of graphene at 300 K. In 2D simulations, the LTECs are positive and does not show any system size dependence. The LTECs obtained from 3D simulations all are negative and shows a system size dependence. The data has been compared with the experiments. <sup>a</sup>Reference<sup>31</sup>, <sup>b</sup>Reference<sup>28</sup>, <sup>c</sup>Reference<sup>29</sup>, <sup>d</sup>Reference<sup>30</sup>.

In 3D simulations, the LTEC are negative for all simulation cells. The LTEC also shows a system size dependence and its value for 10×10×1 simulation cell is roughly half of the value of 150×150×1 cell (table I). The value of LTEC at 300 K ( $\alpha_a = -4.35 \times 10^{-6} K^{-1}$ ) is in qual-

itative agreement with previous calculations<sup>24,25,27</sup>. All simulations predict the LTEC roughly half of the experimental value<sup>28,30</sup> (table I). Unlike DFPT calculations, present study incorporated the full anharmonicity of interatomic potential, hence the disagreement with exper-



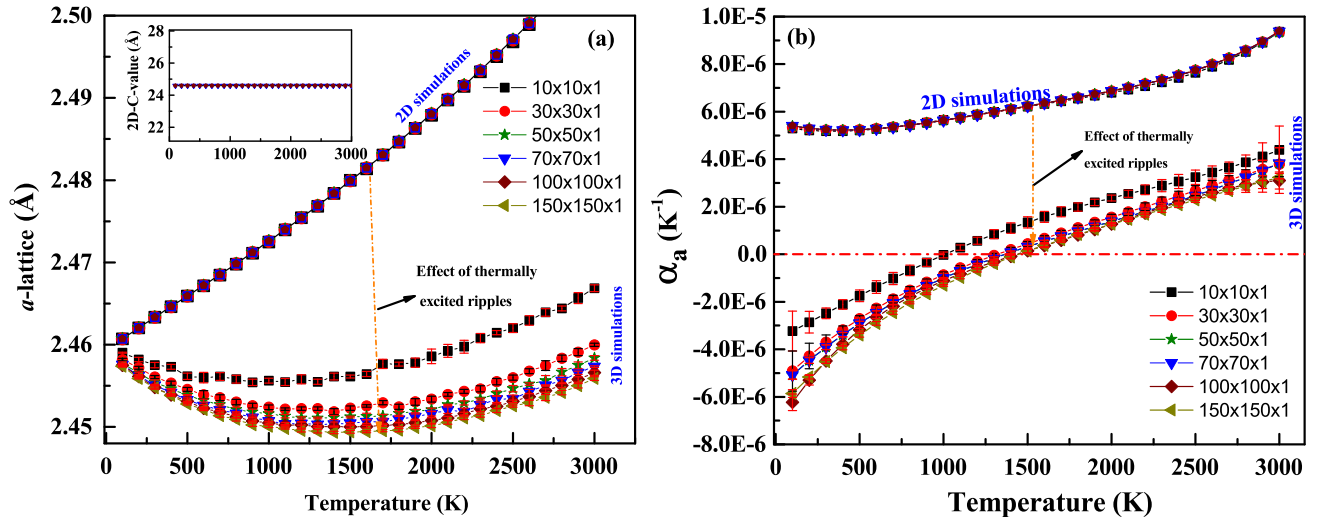


Figure 2. (a) The temperature evolution of in-plane lattice parameter ( $a$ -lattice) of graphene obtained from 2D and 3D simulations. (Inset) C-value obtained from 2D simulations, which doesn't change with temperature. (b) The linear thermal coefficients (LTECs) as a function of temperature. In 3D simulations, the LTEC changes its sign from negative to positive in the temperature range of 1100 K - 1400 K (depends on system size).

imental data may not be due to the strong anharmonic nature of graphene. Though the above experiments<sup>28,30</sup> has taken care to eliminate the strain effect induced by substrate, more accurate analysis is needed to get a clear picture. To support the above arguments, we can see the previous observation of Pozzo *et al*<sup>26</sup>, when the graphene sheet was supported on Ir (111) substrate, it shows thermal expansion instead of thermal contraction. Jiang *et al*<sup>34</sup> used Green's function technique and reported that the LTEC is very sensitive to substrate layer interaction, a weak substrate-layer interaction can cause a significant change in the value of LTEC, and if the substrate effects are strong enough, the LTEC can become positive in the whole computed temperature range. Later, Pan *et al*<sup>31</sup>, used temperature dependent Raman spectroscopy and measured a lower bound of LTEC (at 300 K ( $\alpha_a = -5.5 \times 10^{-6} K^{-1}$ )) of graphene which was supported on BN, while Bao *et al*<sup>28</sup> and Yoon *et al*<sup>30</sup> used Si and SiO<sub>2</sub> substrates to support their graphene sheet, respectively; this may be one of the reason to have different LTEC in these experiments. Our results, along with the earlier theoretical predictions<sup>24,25,27</sup> are in qualitative agreement with Pan *et al*<sup>31</sup>.

The temperature dependence of  $a$ -lattice obtained from 2D simulations is shown in Figure 1. In contrast to 3D simulations,  $a$ -lattice increases with an increase in temperature, and it does not show any system size dependence. Unlike 3D simulations, the LTEC obtained from 2D simulations are all positive in sign and does not have any system size dependence (table I). Since there is no movement of atoms along Z direction, rippling effects are absent in 2D simulations, hence  $a$ -lattice shows a thermal expansion, and the sign of LTEC is positive in the whole computed temperature range. From above ob-

servations, it can be concluded that, the long wavelength ripples are responsible for thermal contraction of free-standing graphene over a wide range of temperatures.

2D h-BN is another one-atom thick material, being 2D crystal, ripples are un-avoidable in 2D h-BN also; hence we extended the above analysis to 2D h-BN to understand its thermal expansion behaviour. The interaction between the B and N atom is modeled using a Tersoff type potential parametrized by Sevik *et al*<sup>35</sup>. The present potential predicts the structural and mechanical properties of 2D h-BN reasonably accurately. The equilibrium  $a$ -lattice obtained with present potential shows an excellent matching with experiments ( $a_0 = 2.500 \text{ \AA}$ )<sup>36,37</sup>. Figure 3 displays the temperature dependence of  $a$ -lattice. In 3D simulation,  $a$ -lattice decreases with an increase in temperature in the whole computed range and matching with our previous study<sup>19</sup>. Similar to graphene,  $a$ -lattice shows a system size dependence in 2D h-BN also, and again we found a convergence from the simulation cell of size  $70 \times 70 \times 1$  (9800) onwards. Paszkowicz *et al*<sup>38</sup> measured the thermal expansion (10 K - 297.5 K) of bulk h-BN using synchrotron X-ray diffraction technique, and they found that  $a$ -lattice shows a flat variation at low temperatures (10 K - 100 K), above 100 K it falls with an increase in temperatures upto 300 K. In 2D simulation, the  $a$ -lattice increases with an increase in temperature and shows thermal expansion in the whole computed temperature range. The  $a$ -lattice does not show any system size dependence in 2D simulations and it is consistent with our observations in graphene. The LTEC obtained at 300 K are shown in table II, the system size dependence of LTEC is discernible. The LTEC at 300 K ( $\alpha_a = -5.509 \times 10^{-6} K^{-1}$ ) is matching with previous quasi-harmonic predictions<sup>27</sup>. The LTEC obtained from

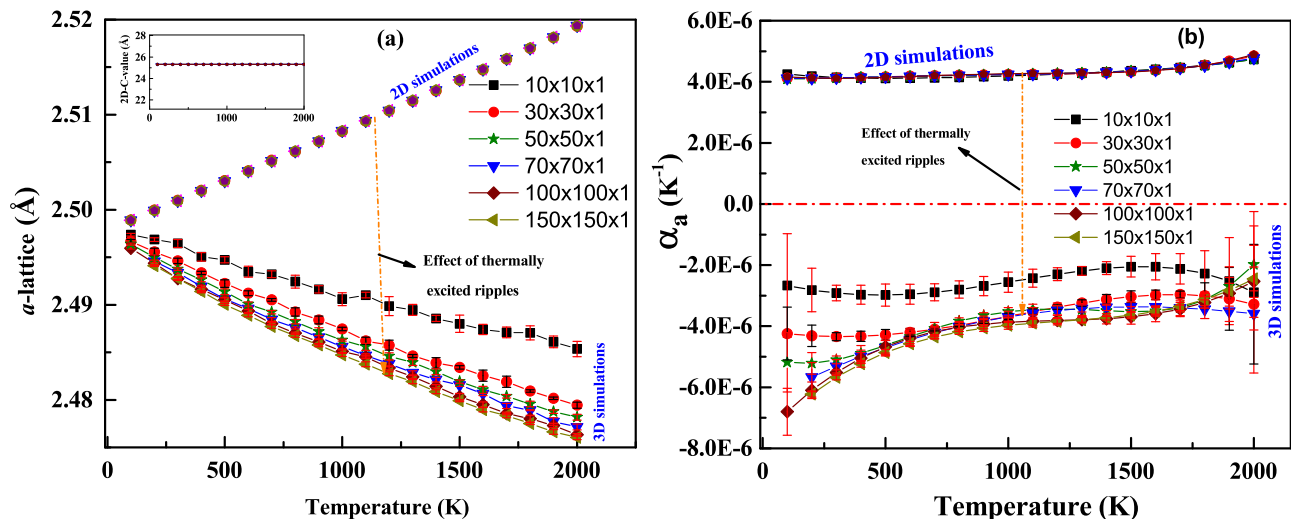


Figure 3. (a) The temperature dependence of in-plane lattice parameter of ( $a$ -lattice) of 2D h-BN; (b) Linear thermal expansion coefficients (LTECs) as a function of temperature

2D simulations all are positive in sign and does not have any system size dependence. Like graphene, the effect of ripples are quite strong in 2D h-BN also, since the empirical potential used to study 2D h-BN and graphene are different, we are not attempting a direct comparison among their data.

Apart from graphene and 2D-h-BN, ML-MoS<sub>2</sub> is another high interesting honeycomb material. The Mo atom layer sandwiched in between two S atom layers (S-Mo-S sandwich structures) in a trigonal prismatic fashion (Figure 1). Liang *et al*<sup>39</sup> parametrized a many body reactive empirical bond order (REBO) potential for Mo-S system. This potential could successfully model the structural and mechanical properties of Mo-S and MoS<sub>2</sub> systems. Later, Stewart and Spearot<sup>40</sup> refined the parametrization and implemented it into MD simulation package LAMMPS. We used the parametrization of Stewart and Spearot<sup>40</sup> to model the interaction between the Mo and S atoms in ML-MoS<sub>2</sub>. The present potential predicts the equilibrium  $a$ -lattice,  $a_0 = 3.17$  Å which is close to the experimentally reported value (3.16 Å)<sup>41</sup>. Figure 4 displays the thermal expansion of  $a$ -lattice and LTEC. The  $a$ -lattice is expanding in the whole computed temperature range in both 2D and 3D simulations, and its system size dependence is marginal. The LTECs of ML-MoS<sub>2</sub> is positive in both 2D and 3D simulations (table III), and their magnitudes are slightly higher in 2D simulations at low temperatures ( $T < 300$  K). The LTEC obtained from 3D simulation at 300 K ( $4.140 \times 10^{-6} K^{-1}$ ) matches with previous experimental data ( $4.922 \times 10^{-6} K^{-1}$ )<sup>42</sup>. Though ML-MoS<sub>2</sub> possess the same hexagonal honeycomb lattice structure of graphene and 2D h-BN, the  $a$ -lattice shows a positive thermal expansion<sup>27,43,44</sup> and it has been measured earlier in bulk-MoS<sub>2</sub> using X-ray powder diffraction<sup>42,45</sup>. This contradiction with graphene and 2D h-BN can be visualized

as an effect of S-Mo-S sandwich structure in ML-MoS<sub>2</sub>, which reduces the rippling behavior considerably<sup>46</sup>. The Mo-Mo distance in Mo layer is higher than that of C-C atom in graphene, hence the Mo-S interaction is responsible for lower height fluctuation of Mo atom in ML-MoS<sub>2</sub><sup>46</sup>. This difference in thermal expansion property among the above mentioned honeycomb materials can be utilized to make future hybrid nano-devices.

In order to understand the underlying mechanism behind the thermal contraction or expansion of solids, Grüneisen theory has been widely used<sup>24,27,47</sup>. According to Grüneisen theory, modes with positive Grüneisen parameters will encourage the thermal expansion, while modes with negative Grüneisen parameter will aid thermal contraction. A solid will undergo thermal expansion or contraction is determined by the balance between the modes with positive and negative Grüneisen parameters<sup>47</sup>. For graphene, the Grüneisen parameters of low lying bending mode (ZA) become large negative (as low as -80). At low temperature only low frequency acoustic modes will be excited, (high frequency optic modes with positive Grüneisen parameters are frozen) and contributes to thermal contraction<sup>24,27</sup>. The negative Grüneisen parameter of ZA mode is due to the membrane effect, predicted by Lifshitz<sup>48</sup>. Apart from graphene, Sevik *et al*<sup>27</sup> extended Grüneisen theory analysis to 2D h-BN and ML-MoS<sub>2</sub>, and they observed a large negative Grüneisen parameter of ZA modes in 2D h-BN also, and it is responsible for thermal contraction. For ML-MoS<sub>2</sub>, the Grüneisen parameter associated with ZA mode is relatively small ( $\sim -10$ ), and leads to thermal contraction only at very low temperature ( $T < 20$  K)<sup>43</sup>. MD simulations are not meaningful at very low temperatures, due to the manifestation of quantum effects. Hence, we performed simulations for temperatures  $T > 100$  K, so we couldn't observe above thermal contraction effects in ML-

| simulation<br>cell size                 | 2D simulation<br>$\alpha_a (\times 10^{-6} K^{-1})$ | 3D simulation<br>$\alpha_a (\times 10^{-6} K^{-1})$ |
|---|---|---|
| $10 \times 10 \times 1$ (200 atoms)     | 4.145   | -2.940  |
| $30 \times 30 \times 1$ (1800 atoms)    | 4.130   | -4.272  |
| $50 \times 50 \times 1$ (5000 atoms)    | 4.124   | -5.151  |
| $70 \times 70 \times 1$ (9800 atoms)    | 4.129   | -5.508  |
| $100 \times 100 \times 1$ (20000 atoms) | 4.114   | -5.509  |
| $150 \times 150 \times 1$ (45000 atoms) | 4.107   | -5.670  |

Table II. The linear thermal expansion coefficients (LTECs) of 2D h-BN at 300 K, the system size dependence of LTECs obtained from 3D simulations are discernible.

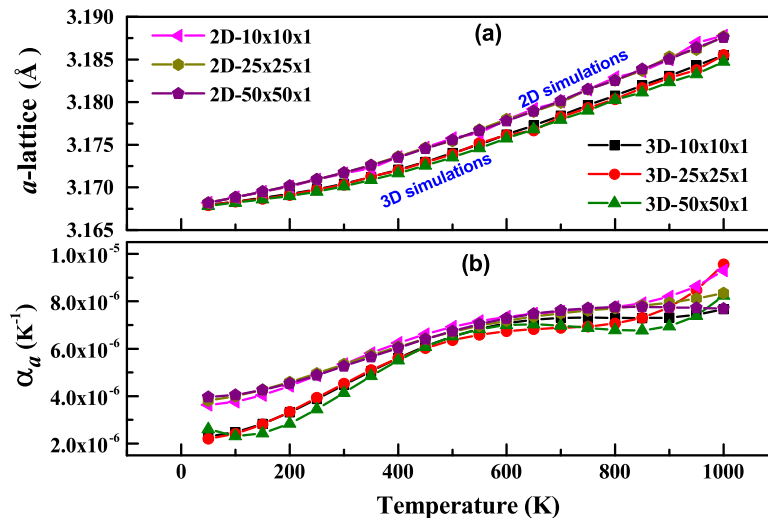


Figure 4. (a) Variation of in-plane lattice parameter ( $a$ -lattice) of ML-MoS<sub>2</sub> with temperature; (b) The linear thermal expansion coefficients (LTECs) as a function of temperature. Unlike graphene and 2D-h-BN, the system size dependence of  $a$ -lattice is marginal in ML-MoS<sub>2</sub>.

MoS<sub>2</sub>. The Grüneisen parameter of ZA is fully negative in graphene<sup>24</sup>, while in ML-MoS<sub>2</sub> it is negative only near the  $\Gamma$  point and becomes positive along K-M direction in the Brillouin zone<sup>43</sup>. This negative-to-positive change attributes to phononic hybridization and finite thickness effects of ML-MoS<sub>2</sub> which counteracts the membrane effects in 2D systems<sup>43</sup>.

The mode dependent Grüneisen parameters are computed by strain derivative of phonon frequencies which obtained using quasi-harmonic approximation (QHA)<sup>24</sup>. One drawback of above method is that, under certain compressive strain, it is difficult to keep the crystal stable. When compressive strain is large enough, it leads to imaginary frequencies around the  $\Gamma$  point which cannot be used to compute the mode Grüneisen parameters. Due to above limitation, wavevectors are computed with less accurate finite difference algorithm around the  $\Gamma$  point<sup>49</sup>. Moreover in QHA we are using a flat 2D sheet, which is devoid of ripples. Despite the above limitations, Grüneisen theory predicts the thermal expansion of honeycomb structures reasonably well.

Instead of Grüneisen theory, here we analyzed the role of different phonon modes on thermal expansion behavior by computing the phonon dispersion at finite tem-

peratures. In order to understand the effect of ripples on phonon modes, one has to compute the phonon dispersion separately from 2D and 3D simulations. Lattice dynamics (LD) methods<sup>50</sup> predicts the phonon frequencies and polarizations from the second derivative of interatomic potential at 0 K, hence it won't make any difference between 2D and 3D simulations, moreover anharmonic effects are completely absent in LD methods. To overcome the above limitation, we developed a spectral energy density based method to compute the phonon frequencies directly from classical MD simulations<sup>18,19</sup>, it will capture the true anharmonic behavior of all phonon modes without any approximations.

Figure 5 shows the 2D phonon dispersion of above mentioned honeycomb structures. The green dot-dash curve is obtained using LD method at 0K, the thick black curve is computed directly from MD simulation. The 3D phonon dispersions of graphene and 2D h-BN at finite temperatures are reported in our earlier papers<sup>18,19</sup>, hence here we are focusing on 2D phonon dispersion at 300 K. The graphene and 2D h-BN unitcell contains 2 basis atom, which leads to six modes of vibrations, three of them are acoustic (A) and remaining three are optic (O) modes. The modes are labeled according to their po-

| simulation<br>cell size              | 2D simulation<br>$\alpha_a (\times 10^{-6} K^{-1})$ | 3D simulation<br>$\alpha_a (\times 10^{-6} K^{-1})$ |
|--------------------------------------|---|---|
| $10 \times 10 \times 1$ (300)        | 5.340   | 4.469   |
| $25 \times 25 \times 1$ (1875 atoms) | 5.343   | 4.530   |
| $50 \times 50 \times 1$ (7500 atoms) | 5.261   | 4.140   |

Table III. The LTECs of ML-MoS<sub>2</sub> at 300 K. The system size dependence of LTECs in both 3D and 2D simulations are insignificant.

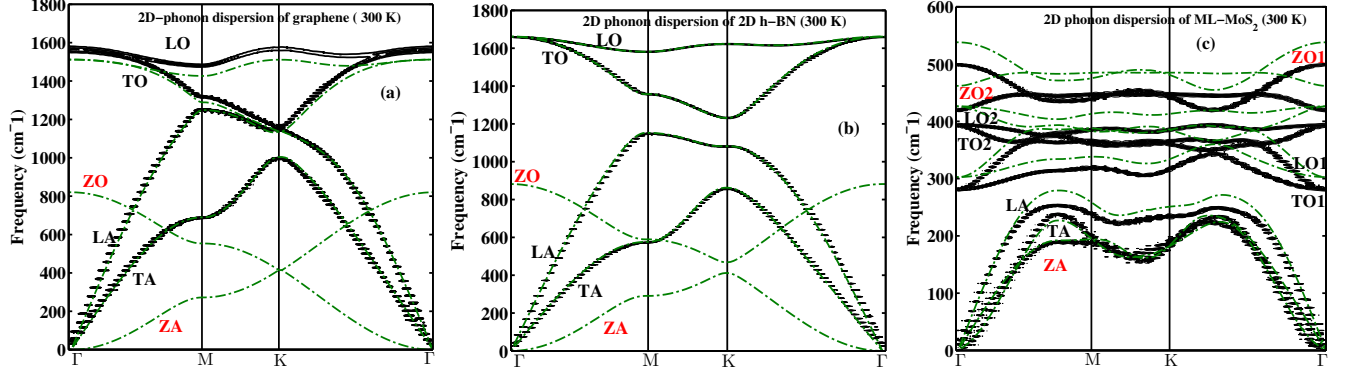


Figure 5. The phonon dispersion of (a) graphene, (b) 2D h-BN and (c) ML-MoS<sub>2</sub>. The green-dot-dash lines are obtained from lattice dynamics calculations (LD) at 0 K, the thick black line is computed directly from 2D-molecular dynamics simulations at 300 K. The out-of-plane modes (ZA, ZO) are absent in 2D phonon dispersion (obtained from MD simulations) of graphene and 2D-h-BN, as a results of constraining the out-of-plane motion. In ML-MoS<sub>2</sub>, all modes are present in both LD and 2D phonon dispersion curves, this attributes to its finite thickness effects

larizations, the letter 'L', 'T', and 'Z' are used to denote longitudinal, transverse and out-of-plane modes respectively. The ZA mode shows a quadratic dispersion in graphene and 2D h-BN, which is a characteristic feature of layered compounds<sup>48</sup>, and it is due to  $D_{3h}$  point group symmetry<sup>51</sup>. The Overall agreement of LD frequencies of graphene and h-BN with previous calculations are satisfactory<sup>35,52</sup>. In 2D dispersion, the in-plane acoustic modes LA and TA shows similar behavior as reported in 3D dispersion<sup>18,19</sup>. The most interesting phenomena observed here is the absence of out-of-plane modes such as ZA and ZO in 2D phonon dispersions of both graphene and 2D h-BN. Since we arrested the motion of atoms along Z directions, the branches corresponding to out-of-plane motions are missing in phonon dispersion. This complete absence of ZA and ZO mode is the reason behind the continuous thermal expansion of  $a$ -lattice in 2D simulations, and this observation is completely agreeing with Grüneisen theory based analysis. The novelty of the present approach is that, it exposes the importance of out-of-plane modes (ZA) in determining the thermal expansion behavior, by computing the phonon dispersion from the typical dynamics of atoms, instead of symmetry based LD methods.

In ML-MoS<sub>2</sub>, due to the trigonal prismatic arrangement of Mo and S atoms, vibrational modes behaves quite differently from graphene and 2D h-BN. The unitcell of ML-MoS<sub>2</sub> contains three basis atoms, hence there will be nine modes of vibrations (3 acoustic+6 optic). Figure 5c

displays the phonon dispersion in h-MoS<sub>2</sub>. The LD calculations are in good agreement with previous reports<sup>53,54</sup>. The gap between the acoustic and optic mode (TO1) is discernible, where three acoustic branches TA, LA and ZA are separated below the optic branch (TO1) by  $\sim 55$   $\text{cm}^{-1}$  at M point in the Brillouin zone, and it is in agreement with *ab initio* calculations<sup>53</sup>. The LA and TA modes show linear dispersion, while ZA mode exhibits quadratic dispersion around the  $\Gamma$  point, analogous to graphene and h-BN. Unlike graphene and h-BN, all out-of-plane modes are present in 2D dispersion of ML-MoS<sub>2</sub>. Though we arrested the out-of-plane motion, the ZA and ZO branches are still persisting in ML-MoS<sub>2</sub>, and this can be ascribed to the finite thickness effect of ML-MoS<sub>2</sub>. The graphene and h-BN are one atom thick structure and have more flexibility along out-of-plane direction, the S-Mo-S sandwich structure of ML-MoS<sub>2</sub> makes it a more rigid material along out-of-plane direction and leads to less rippling. The magnitude of thermally excited ripples can be quantified using the height-height correlation function  $\langle h^2 \rangle$ , and its value is much smaller for ML-MoS<sub>2</sub> in comparison with graphene, and it is an outcome of less rippling behaviour of ML-MoS<sub>2</sub><sup>46</sup>. The finite thickness of ML-MoS<sub>2</sub> counteracts the membrane effects, and hence the origin of bending mode (ZA) is not purely due to the out-of-plane vibrations as in graphene and h-BN.



#### IV. CONCLUSIONS

Thermally excited ripples are inevitable in 2D crystals, and they can affect the thermo-physical properties of these materials significantly. In order to delineate the role of ripples on thermal expansion of 2D honeycomb materials (graphene, 2D h-BN and ML-MoS<sub>2</sub>) we performed three-dimensional (3D) and two dimensional (2D) molecular dynamics simulations, the later cannot incorporate the effects of ripples. The in-plane lattice parameter ( $\mathbf{a}$ -lattice) of free-standing graphene calculated from 3D simulations shows a thermal contraction upto  $T = 1300\text{ K} - 1400\text{ K}$  (depend on system size) and expands thereafter. The linear thermal expansion coefficient (LTEC) changes its sign from negative to positive in the above temperature range. At the same time, the  $\mathbf{a}$ -lattice of very same system obtained from 2D simulations shows continuous thermal expansion instead of thermal

contraction and LTECs are positive for all system sizes. The above analysis was extended to 2D h-BN and found the similar discrepancy between 2D and 3D simulations. Contradicting to graphene and 2D h-BN, the  $\mathbf{a}$ -lattice of ML-MoS<sub>2</sub> shows thermal expansion in both 3D and 2D simulations, and the LTECs are positive and their system size dependence is marginal. The above discrepancy is analyzed by computing the 2D phonon dispersion at 300 K using spectral energy density method. The out-of-plane bending (ZA) mode is missing in 2D phonon dispersions of graphene and 2D h-BN. The ZA mode, which is responsible for thermal contraction of in-plane lattice parameter at low temperature is absent in 2D simulations, which leads to continuous thermal expansion. However, these modes are present in 2D dispersion of ML-MoS<sub>2</sub>, indicates that its origin is not purely due to the out-of-plane vibrations, and its effects on thermal expansion is not significant as found in graphene and 2D h-BN systems.

- 
- \* [anees@igcar.gov.in](mailto:anees@igcar.gov.in)  
 † [mc.valsakumar@gmail.com](mailto:mc.valsakumar@gmail.com)  
 ‡ [bkp@igcar.gov.in](mailto:bkp@igcar.gov.in)
- <sup>1</sup> A. K. Geim and K. S. Novoselov, *Nature materials* **6**, 183 (2007).
  - <sup>2</sup> A. A. Balandin, *Nature materials* **10**, 569 (2011).
  - <sup>3</sup> C. Lee, X. Wei, J. W. Kysar, and J. Hone, *Science* **321**, 385 (2008).
  - <sup>4</sup> F. Schwierz, *Nat Nano* **5**, 487 (2010).
  - <sup>5</sup> A. H. Castro Neto, F. Guinea, N. M. R. Peres, K. S. Novoselov, and A. K. Geim, *Rev. Mod. Phys.* **81**, 109 (2009).
  - <sup>6</sup> D. Golberg, Y. Bando, Y. Huang, T. Terao, M. Mitome, C. Tang, and C. Zhi, *ACS Nano* **4**, 2979 (2010).
  - <sup>7</sup> Y. Shi, C. Hamsen, X. Jia, K. K. Kim, A. Reina, M. Hofmann, A. L. Hsu, K. Zhang, H. Li, Z.-Y. Juang, et al., *Nano Letters* **10**, 4134 (2010).
  - <sup>8</sup> K. Watanabe, T. Taniguchi, and H. Kanda, *Nat Mater* **3**, 404 (2004).
  - <sup>9</sup> A. K. Geim and I. V. Grigorieva, *Nature* **499**, 419 (2013).
  - <sup>10</sup> M. Chhowalla, H. S. Shin, G. Eda, L.-J. Li, K. P. Loh, and H. Zhang, *Nat Chem* **5**, 263 (2013).
  - <sup>11</sup> X. Huang, Z. Zeng, and H. Zhang, *Chem. Soc. Rev.* **42**, 1934 (2013).
  - <sup>12</sup> A. Splendiani, L. Sun, Y. Zhang, T. Li, J. Kim, C.-Y. Chim, G. Galli, and F. Wang, *Nano Letters* **10**, 1271 (2010).
  - <sup>13</sup> RadisavljevicB, RadenovicA, BrivioJ, GiacomettiV, and KisA, *Nat Nano* **6**, 147 (2011).
  - <sup>14</sup> S.-W. Min, H. S. Lee, H. J. Choi, M. K. Park, T. Nam, H. Kim, S. Ryu, and S. Im, *Nanoscale* **5**, 548 (2013).
  - <sup>15</sup> J. Na, M.-K. Joo, M. Shin, J. Huh, J.-S. Kim, M. Piao, J.-E. Jin, H.-K. Jang, H. J. Choi, J. H. Shim, et al., *Nanoscale* **6**, 433 (2014).
  - <sup>16</sup> N. D. Mermin, *Phys. Rev.* **176**, 250 (1968).
  - <sup>17</sup> A. Fasolino, J. Los, and M. I. Katsnelson, *Nature materials* **6**, 858 (2007).
  - <sup>18</sup> P. Anees, M. C. Valsakumar, and B. K. Panigrahi, *2D Materials* **2**, 035014 (2015).
  - <sup>19</sup> P. Anees, M. C. Valsakumar, and B. K. Panigrahi, *Phys. Chem. Chem. Phys.* **18**, 2672 (2016).
  - <sup>20</sup> J. C. Meyer, A. K. Geim, M. I. Katsnelson, K. S. Novoselov, T. J. Booth, and S. Roth, *Nature* **446**, 60 (2007).
  - <sup>21</sup> P. Gallagher, M. Lee, F. Amet, P. Maksymovych, J. Wang, S. Wang, X. Lu, G. Zhang, K. Watanabe, T. Taniguchi, et al., *ArXiv e-prints* (2015).
  - <sup>22</sup> V. M. Pereira and A. H. Castro Neto, *ArXiv e-prints* (2008).
  - <sup>23</sup> D. C. Elias, R. R. Nair, T. M. G. Mohiuddin, S. V. Morozov, P. Blake, M. P. Halsall, A. C. Ferrari, D. W. Boukhvalov, M. I. Katsnelson, A. K. Geim, et al., *Science* **323**, 610 (2009).
  - <sup>24</sup> N. Mounet and N. Marzari, *Phys. Rev. B* **71**, 205214 (2005).
  - <sup>25</sup> K. V. Zakharchenko, M. I. Katsnelson, and A. Fasolino, *Phys. Rev. Lett.* **102**, 046808 (2009).
  - <sup>26</sup> M. Pozzo, D. Alfè, P. Lacovig, P. Hofmann, S. Lizzit, and A. Baraldi, *Phys. Rev. Lett.* **106**, 135501 (2011).
  - <sup>27</sup> C. Sevik, *Phys. Rev. B* **89**, 035422 (2014).
  - <sup>28</sup> W. Bao, F. Miao, Z. Chen, H. Zhang, W. Jang, C. Dames, and C. N. Lau, *Nat Nano* **4**, 562 (2009).
  - <sup>29</sup> V. Singh, S. Sengupta, H. S. Solanki, R. Dhall, A. Allain, S. Dhara, P. Pant, and M. M. Deshmukh, *Nanotechnology* **21**, 165204 (2010).
  - <sup>30</sup> D. Yoon, Y.-W. Son, and H. Cheong, *Nano Letters* **11**, 3227 (2011).
  - <sup>31</sup> W. Pan, J. Xiao, J. Zhu, C. Yu, G. Zhang, Z. Ni, K. Watanabe, T. Taniguchi, Y. Shi, and X. Wang, *Scientific Reports* **2**, 893 EP (2012).
  - <sup>32</sup> S. Plimpton, *Journal of Computational Physics* **117**, 1 (1995), URL <http://lammps.sandia.gov>.
  - <sup>33</sup> J. H. Los and A. Fasolino, *Phys. Rev. B* **68**, 024107 (2003).
  - <sup>34</sup> J.-W. Jiang, J.-S. Wang, and B. Li, *Phys. Rev. B* **80**, 205429 (2009).
  - <sup>35</sup> C. Sevik, A. Kinaci, J. B. Haskins, and T. Çağ m, *Phys. Rev. B* **84**, 085409 (2011).



- <sup>36</sup> D. Pacilé, J. C. Meyer, Ç. Ö. Girit, and A. Zettl, *Applied Physics Letters* **92**, 133107 (2008).
- <sup>37</sup> A. Nag, K. Raidongia, K. P. S. S. Hembram, R. Datta, U. V. Waghmare, and C. N. R. Rao, *ACS Nano* **4**, 1539 (2010).
- <sup>38</sup> W. Paszkowicz, J. Pelka, M. Knapp, T. Szyszko, and S. Podsiadlo, *Applied Physics A* **75**, 431 (2002).
- <sup>39</sup> T. Liang, S. R. Phillpot, and S. B. Sinnott, *Phys. Rev. B* **79**, 245110 (2009).
- <sup>40</sup> J. A. Stewart and D. E. Spearot, *Modelling and Simulation in Materials Science and Engineering* **21**, 045003 (2013).
- <sup>41</sup> C. Ataca, M. Topsakal, E. Aktürk, and S. Ciraci, *The Journal of Physical Chemistry C* **115**, 16354 (2011).
- <sup>42</sup> R. Murray and B. Evans, *Journal of Applied Crystallography* **12**, 312 (1979).
- <sup>43</sup> L. F. Huang, P. L. Gong, and Z. Zeng, *Phys. Rev. B* **90**, 045409 (2014).
- <sup>44</sup> P. Anees, M. C. Valsakumar, and B. K. Panigrahi, *Applied Physics Letters* **108** (2016).
- <sup>45</sup> S. H. El-Mahalawy and B. L. Evans, *Journal of Applied Crystallography* **9**, 403 (1976).
- <sup>46</sup> S. K. Singh, M. Neek-Amal, S. Costamagna, and F. M. Peeters, *Phys. Rev. B* **91**, 014101 (2015).
- <sup>47</sup> P. K. Schelling and P. Keblinski, *Phys. Rev. B* **68**, 035425 (2003).
- <sup>48</sup> M. Lifshitz, *Zh. Eksp. Teor. Fiz.* **22**, 475 (1952).
- <sup>49</sup> L. Karssemeijer and A. Fasolino, Master's thesis, *Theory of Condensed Matter*, Institute for Molecules and Materials, Radboud University Nijmegen (2010).
- <sup>50</sup> M. T. Dove, *Introduction to Lattice Dynamics* (Cambridge University Press, 1993).
- <sup>51</sup> G. D. R. Saito and M. Dresselhaus, *Physical Properties of Carbon Nanotubes* (London: Imperial College Press, 1998).
- <sup>52</sup> L. Karssemeijer and A. Fasolino, *Surface Science* **605**, 1611 (2011).
- <sup>53</sup> Y. Cai, J. Lan, G. Zhang, and Y.-W. Zhang, *Phys. Rev. B* **89**, 035438 (2014).
- <sup>54</sup> A. Molina-Sánchez and L. Wirtz, *Phys. Rev. B* **84**, 155413 (2011).